PERFORMANCE ASSESSMENT OF NONLINEAR DYNAMIC ACTUATOR MODEL USING DRY WIND TUNNEL TEST

M. Tang, M. Böswald
German Aerospace Center, AE-SAS, Bunsenstr. 10, Göttingen, Germany

Abstract

Active control in aeroelasticity has gained more interest recently. Actuator performance is highly sensitive to the overall performance of aero-servo-elastic systems. However, actuators themselves can be considered as dynamic systems and dynamic substitute models for actuators are needed in the design of aero-servo-elastic systems. In this paper, it is investigated if a nonlinear actuator model can lead to better performance prediction of the aero-servo-elastic system, especially when control commands provoke nonlinear actuator behavior. The research is being conducted from the perspective of active flutter suppression. With increasing flight speed, some eigenmodes of the systems may feature a decrease of damping. Control surface actuators shall be used to counteract this aeroelastic effect. For a first proof of concept, a simple experiment is being conducted. Instead of using a wind tunnel, a hybrid numerical and experimental simulation environment is set up to emulate wind on conditions for a laboratory model (dry wind tunnel test). Within this environment, the performance of an actuator with nonlinear behavior is analyzed and compared to simulations.

Keywords

Aeroservoelasticity; Actuator; Flutter Suppression

NOMENCLATURE

Symbols

D	damping ratio	-
d	damping coefficient	kg/s
F	force	N
F_e	inertial excitation	N
k	stiffness	N/m
M	mass	kg
m	control surface mass	kg
μ	modal mass	-
ω_0	eigenfrequency	rad/s
Ω	excitation frequency	rad/s
φ	control surface angular deflection	deg
p_I	control gain shaker	-
r	distance center of gravity control surface to wing	m
u	system input	N
p_F	control gain flap	-
x	wing deflection	m
x_2	control surface deflection	m

1. INTRODUCTION

One major goal for future aircraft design is reduction of fuel consumption and emissions. In order to achieve this goal, weight of the overall aircraft has to be reduced, among others. Lightweight structures however are prone to vibrations. Thus, interaction of dynamic structural deformation and unsteady aerodynamics are becoming more important. These effects and corresponding technologies are being investigated in the field of aeroelasticity. One major aeroelastic effect is the so-called flutter phenomenon. This leads to unstable vibrations of the airframe with growing amplitudes which stresses the structural components and make the vehicle uncontrollable. For obvious reasons, flutter must be avoided within the entire flight envelope and slightly beyond. With the tendency to high aspect ratio wings and thus more flexible aircraft, this might lead to undesired limitations of the flight envelope.

Of course, the occurrence of flutter can be pushed outside the envelope by design adaptations of the flight vehicle. These design adaptations may consist of mass or stiffness modification which will lead to an increase of weight, which is also undesirable for different reasons. Another possibility is the use of active flutter suppression in order to stabilize the system [1, 2]. This means that the occurrence of flutter is possible within the flight envelope, but stability is maintained by an active control system (i.e. active flutter suppression). In order to achieve this,

measurements of the aircraft dynamic response and an actuator to actively control the aircraft response is needed. Finally, a smart control algorithm is required which can handle the parameter-varying character of a flight vehicle and which is robust to ensure proper operation with least likelihood of failure.
The control algorithm is designed with a priori knowledge about the aeroelastic system, i.e. the structural dynamics and unsteady aerodynamics of the aircraft. Also, the behavior of the actuator is essential for the controller [3]. State of the art controller design assumes linear time-invariant systems, nevertheless, the structure may respond nonlinear, for example due to friction, aerodynamics cause nonlinear behavior in the transonic regime. The actuator saturates, when commanded signals are not reachable, for example due to rate limits and therefor become nonlinear. This work investigates the influence of the nonlinear actuator on the control performance.
To study the effect of actuator nonlinearity on the overall performance of aero-servo-elastic systems experimentally, unsteady aerodynamics is required and thus a flying demonstrator or at least a wind tunnel test is needed, although only the actuator behavior is of interest. In order to test the system in an early conceptual phase, the idea of dry wind tunnel tests has been utilized [4, 5]. Shakers are used to emulate the effect of deformation induced unsteady aerodynamic forces acting on the mechanical system. A controller computes aerodynamic forces from measured displacements of the structure and provides the electric drive signals for the shakers. Next to the dynamic response of the structure, the controller is also fed with quasi-steady input signals proportional to flight speed and flight altitude. This active control setup enables to investigate the onset of flutter in a ground test without airflow. But instead of using this setup for linear flutter stability assessment on ground, it will rather be used to investigate the performance of actively controlled system with a control surface actuator. While the external shakers with active control are being used to emulate the unsteady aerodynamic forces, which can lead to flutter, a control surface actuator shall be used to stabilize the system again. Stabilization in this context means to increase the damping of the aero-elastic-system. Consequently, another active controller (i.e. the active flutter suppression controller) is required, which uses the dynamic response of the structure to compute a drive signal for the control surface actuator. The performance of the overall system with active flutter suppression in a dry wind tunnel setup is being investigated for different operational conditions. Special focus is put on larger response amplitudes, when the control surface actuator is operating in the nonlinear domain.

2. THEORETICAL BACKGROUND

A common setup for flutter suppression is the usage of control surfaces in order to suppress vibrations of the wing. Typically, flutter occurs due to a coupling of two or more modes. For one mode, the damping will increase when approaching the flutter critical speed, whereas the damping of one other mode will decrease. The idea is to focus on the one mode whose damping is being reduced when approaching the flutter point. This can be, for example, a bending mode of the wing that couples with a torsion mode. This will be modeled by a simple one degree of freedom system as shown in Figure 1. The actuator drives a control surface and a single force is applied, representing aerodynamic forces. However, in the dry wind tunnel test setup that is being used here, we do not have aerodynamic forces acting on the control surface. Instead of an aerodynamic force, the control surface introduces inertial forces acting on the mass. Modeling of aerodynamics is kept simple, since it is not scope of this work, so the aerodynamic model is being reduced to a velocity proportional force. This allows to change the system and drive it into an unstable condition. In principle, one stable system should be driven unstable. The equation of motion for the vertical bending oscillation of the wing results in

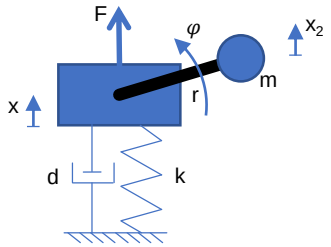

FIG 1. sdof model for wing with control surface

$$M\ddot{x} + d\dot{x} + kx = F + F_e \quad , \tag{1}$$

where M represents the mass, d the damping, k the stiffness, F the external force and F_e the force resulting from the inertia of the control surface. Only the vertical bending motion according to x in Figure 1 is being modeled here. Therefore, the moment of force generated by the inertial force of the control surface is disregarded.
In case of forcing by unsteady aerodynamics, the force depends on the current state of the wing in terms of displacement, velocity and acceleration. Additional internal states, so-called lag states arise if time domain models are derived, e.g. with Rogers approximation. Assuming the control surface is rigid, this results in imbalance excitation proportional to the acceleration of the control surface. In contrast rotor dynamics, where unbalance masses rotate with steady rotation speed, the control surface oscillates harmonically around its nominal angular position. The rotational movement of the control surface and

the first and second time-derivative can be described by the following equations

$$x_2 = x + r\sin\varphi \tag{2}$$

$$\dot{x}_2 = x + r\dot{\varphi}\cos\varphi \tag{3}$$

$$\ddot{x}_2 = x + r\ddot{\varphi}\cos\varphi - r\dot{\varphi}^2\sin\varphi \quad , \tag{4}$$

with r being the distance of the center of gravity of the flap from the hinge line, φ the angular deflection of the control surface and x the vertical deflection of the wing. The second term in equation (4) refers to the Euler force and the third term refers to the centrifugal force. The radius r is assumed constant, otherwise an additional term for the Coriolis force would appear. Assuming the commanded deflection of the control surface being a harmonic function $\varphi = \varphi_0\cos(\Omega t)$ with small angular deflections, some assumptions can be made.
The cosine term in the Euler force is approximately 1 for small amplitudes φ_0. The centrifugal force can be neglected, due to small values computed for small angle and also the result of the squared of a small value. The centrifugal force is approximately two orders of magnitude lower than the Euler force. The inertial forces acting on the wing results in

$$F_e = m\ddot{x}_2 = m\left(\ddot{x} + r\ddot{\varphi}\right) \quad . \tag{5}$$

Inserting this relation into the equation of motion (1) yield the following equation of motion for the vertical bending vibration of the wing. In this case, the force F represents the motion induced unsteady aerodynamic force acting on the system:

$$(M+m)\ddot{x} + d\dot{x} + kx = F + mr\ddot{\varphi} \quad . \tag{6}$$

The current state of the wing can be measured with adequate sensors. The response signals are fed back into a real time controller, computing the external force F with a model representing the unsteady aerodynamics. The intention is not to model unsteady aerodynamics in the dry wind tunnel test as accurate as possible. Instead, only the decreasing damping effect of the unsteady aerodynamic force shall be included in the setup. Therefore, the aerodynamic force is modeled here in a simplified way as velocity proportional force resulting in $F = -p_I\dot{x}$, with p_I as the gain of the controller. The equation of motion for the force controlled system or dry wind system is then

$$M\ddot{x} + d\dot{x} + kx = -p_I\dot{x} - m\left(\ddot{x} + r\ddot{\varphi}\right) \tag{7}$$

$$(M+m)\ddot{x} + (d+p_I)\dot{x} + kx = -mr\ddot{\varphi} \quad . \tag{8}$$

As one can see, the damping term in the equation of motion is governed directly by the control parameter. Consequently, the stability of the system can easily be controlled by variation of this parameter.
The active flutter suppression is implemented as velocity (of the wing) proportional control of the control surface in order to increase damping. However, in this case the angular deflection is commanded and not the angular acceleration. Nevertheless, with harmonic excitation only a factor separates angular acceleration and angular deflection. This means that the active flutter control is ultimately velocity proportional.

$$\varphi = p_F\dot{x} \tag{9}$$

$$\ddot{\varphi} = p_F\dddot{x} \tag{10}$$

$$\ddot{\varphi} = -p_F\Omega^2\dot{x} \quad \text{,for harmonic excitation.} \tag{11}$$

The complete equation of motion with control laws for dry wind and flutter suppression is finally

$$(M+m)\ddot{x} + (d + p_I - p_F\Omega^2)\dot{x} + kx = 0 \quad . \tag{12}$$

Whereas the stability of the system can be decreased by changing the control parameter p_I, the inertial force of the control surface is used to stabilize the system again by increasing the damping, through the control parameter p_F. With proper setting of the p_I parameter, disturbing the wing e.g. by some external impulse will lead to undamped harmonic oscillations representing the onset of flutter during some flight condition. The corresponding inertial force of the control surface (resulting from actively controlled control surface motion) increases the damping of the system and stabilizes the system again which is controlled by the parameter p_F.
The equation of motion can be transformed by Fourier-transformation into the frequency-domain and the transfer function is obtained from the ratio of the response and the input command for the control surface rotation:

$$\frac{x}{\varphi} = \frac{-\Omega^2 mr}{-\Omega^2(M+m) + i\Omega(p_I - p_F\Omega^2) + k} \tag{13}$$

Transformation of the open loop system into the normal form using the expressions for eigenfrequency $\omega_0 = \sqrt{k/(M+m)}$ and damping ratio $2D\omega_0 = d/(M+m)$ yields:

$$\frac{x}{\varphi} = \frac{\frac{m}{M+m}r\Omega^2}{\omega_0^2 + 2iD\omega_0\Omega - \Omega^2} \tag{14}$$

$$\frac{\ddot{x}}{\varphi} = \frac{\frac{m}{M+m}r\Omega^4}{\omega_0^2 + 2iD\omega_0\Omega - \Omega^2} \quad , \tag{15}$$

where the first wing bending is described with its eigenfrequency and damping ratio.
Inserting the equation for the external force excitation yields the following equation for the transfer function:

$$\frac{\ddot{x}}{F} = \frac{\frac{1}{\mu}\Omega^2}{\omega_0^2 + 2iD\omega_0\Omega - \Omega^2} \quad , \tag{16}$$

where μ is the modal mass corresponding to the first wing bending in this case. Equations (15) and (16) are used in order to identify the wing structure experimentally from which the simulation model is built. This represents the open loop system, so that the control loop is integrated separately in the simulation model.

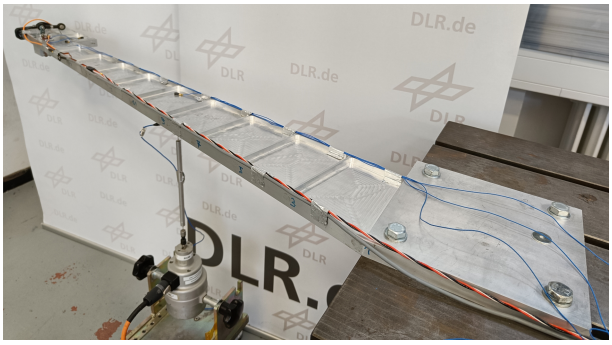

FIG 2. Aluminum wing with shaker and control surface

If physical limitations of the controller are met, controller performance of the flutter suppression will degrade or fail completely, i.e. the control parameter p_F reduces. The influence of those limitations is going to be studied in this work.

3. TEST SETUP

3.1. Experimental Setup

The mechanical structure chosen for this investigation is a structural model of a wing with an actuated control surface. Wing and control surface are manufactured from solid aluminum. The control surface is driven by a servo. The wing is clamped at the root to a foundation. The overall experimental setup is presented in Figure 2. From previous tests, it is known that the first wing bending is at 5.3 Hz. The the next mode is a second wing bending at 41.3 Hz. Those two modes are well separated, so that the first mode can be simplified as a single degree of freedom system. Since the control surface is manufactured from solid aluminum, the corresponding inertial forces are sufficiently high to affect the wing vibrations. A servo is used in order to drive the control surface. It is controlled by digital signals, so called PWM signals, to command the angular displacement of the servo lever. The servo lever is connected to the control surface with a simple rod. The mechanism is designed in such a way that the angular deflection of the servo is identical to the angular deflection of the control surface. The hinge of the control surface and the hinges in the drive mechanism of the control surface are all sliding bearings with just little freeplay.
A small shaker is chosen for force excitation , allowing forces up to 25 N, see Figure 2. A power amplifier is used to drive the shaker, shown in Figure 3 in the bottom picture. One accelerometer is placed in the wing tip area on the wing next to the hinge of the control surface. This accelerometer signal is used to control the shaker (i.e. emulation of aerodynamic forces) and the control surface (i.e. active flutter suppression). Moreover, one potentiometer is mounted on the hinge line of the control surface to monitor its current position. The servo and potentiometer are fed by a DC voltage supply.

FIG 3. Top: ADwin Pro II, IEPE and power source; bottom: amplifier and DAQ

ADwin Pro II is utilized as real time controller with analog inputs, analog outputs and also PWM signals as digital outputs. Figure 3 on the top shows the real time controller. Simulink models can be compiled and deployed on the system to simulate a model representing the unsteady aerodynamics and a controller for the control surface. For unsteady aerodynamics, an integral controller is used to apply time integration on the acceleration data and compute the required velocity proportional signal for the active control. The same control approach is used for the control surface to increase damping and therefor stabilize the wing, if damping becomes negative. Both controls use the same acceleration input from the wing structure.

3.2. Identification

In order to characterize the servo, undesired interaction with elastic vibrations of the wing should be avoided. To achieve this, the wing tip has been clamped but the servo with control surface can freely rotate. This setup can be used to identify the dynamic behavior of the servo with control surface independently, as seen in Figure 4. Because the actual control surface is already mounted to the

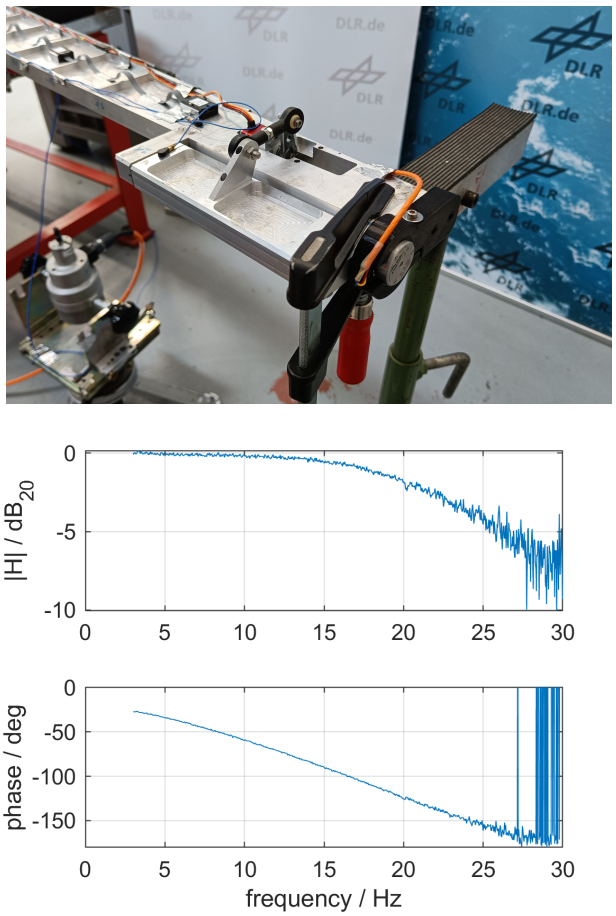

FIG 4. Top: clamped wing tip for actuator identification; bottom: transfer funciton for actuator

servo, operational conditions are representative for this identification process. The free play in the control surface actuation mechanism is estimated with 0.9 deg, the maximum available velocity is measured at 850 deg/s and the highest possible acceleration for the actuator is approximately at 9000 deg/s^2. The cut-off frequency for the servo is identified around 20 Hz. However, the transfer function does not correspond to a first order system, therefore, a higher order transfer function has been applied in order to represent the actuator. In addition, a delay of the actuator is expected. The transfer function is shown in Figure 4 bottom as gain in the upper diagram and phase in the lower diagram. It can be seen there, that the delay yields to a phase lag of 34 deg at 5 Hz, which is significant.

The modal stiffness, modal mass and modal damping of the aluminum wing is identified for the considered first wing bending mode with the shaker but also with control surface excitation. Both excitation points are necessary in order to describe the transfer paths and build a simulation model with measured data, as shown in equations (15) and (16). The first wing bending does have the same dynamics for both inputs but the residue is different due to the different load paths. Since it is simplified as a one degree of freedom system, the residue contains already the transfer path from excitation point to response point.

Figure 5 shows the transfer functions of the wing for the different excitation. On the top, force excitation with the shaker is seen and on the bottom control surface excitation from the actuator is seen, where the response is an accelerometer on the wing structure close to the control surface. The transfer function on the bottom is important for the control design of the active flutter suppression using the control surface and the transfer function on the top is needed to design the shaker control in order to emulate the unsteady aerodynamic forces in the dry wind tunnel concept. It is clearly seen, that the assumption of the single degree of freedom system is valid. Even though the amplitudes of the two transfer functions differ significantly, the pole (i.e. complex eigenvalue) of the system should theoretically remain the same for both excitations, since the structure is still the same. However, slight differences in the pole estimate for both transfer functions are observed when processing the two transfer function with a modal parameter estimator. Also, a delay for the control surface excitation is seen, which can be observed as a linear phase drift and arises from the actuator. Processing this transfer function with a modal parameter estimator might lead to less accurate estimates because it is inconsistent with the assumptions of modal parameter estimation. The eigenfrequency is identified from force excitation at 5.33 Hz and from control surface excitation at 5.31 Hz. Damping from force excitation is estimated at 0.6 % and from control surface excitation at 0.4 %. So the deviations between the two are not too severe. As already stated above, the amplitudes of the two transfer functions are different. This can be explained by different residues from force excitation and control surface excitation. The modal mass from force excitation as stated in equation (16) is computed at 5.05 and the residue (numerator) for control surface excitation as stated in equation (15) is 0.0022. For inertial excitation, the residue consists of several parameters, nevertheless, the resulting numeric value is good enough to represent the system.

Furthermore, the power amplifier for the shaker is characterized by measuring the transfer function from drive signal to force current, shown in Figure 3. For control of the dry wind, the transfer function of the system from drive signal to wing response must be known. This consists of the behavior of the wing as well as the behavior of the amplifier. Surprisingly, the transfer function resembles a high pass filter with a gain of 7.4 N/V and a time constant of 0.3s (3.3 Hz).

In a next step, the shaker control is implemented using the accelerometer as the feed back signal. The unsteady aerodynamics is modeled as simple velocity feedback, so that the system can be driven unstable. Figure 7 shows the measured transfer functions of the laboratory structure. In this experimental model, the effect of the parameter p_I on the overall damping of the system is observed. To this end, transfer functions have been calculated for control surface excitation for different settings of the shaker control parameter p_I. Positive values of p_I should increase damping, while

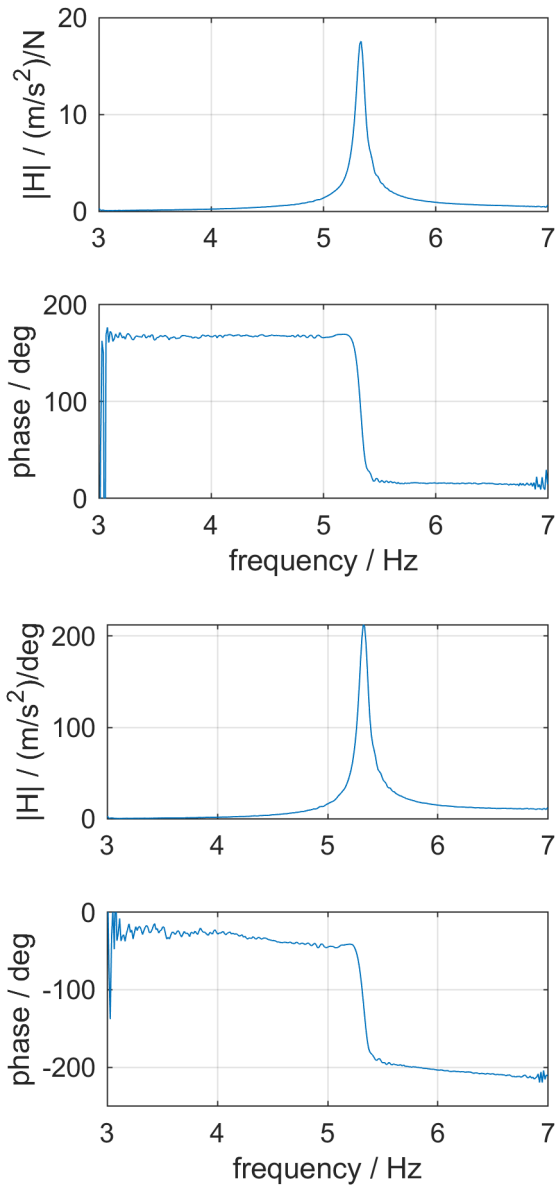

FIG 5. Transfer functions of the wing. Top: force excitation, bottom: control surface excitation

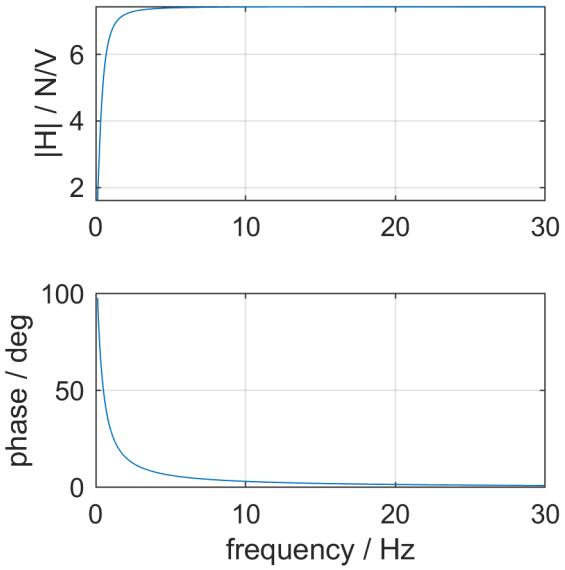

FIG 6. transfer function of amplifier

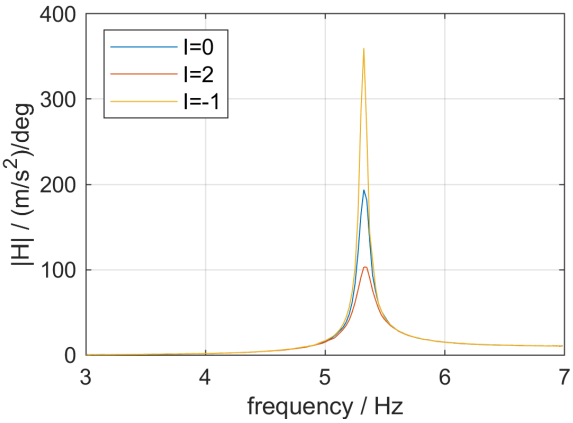

FIG 7. Measured transfer function for dry wind tests with control surface excitation

negative values should decrease the system damping. The damping for the open loop system without control is identified at 0.4 % (i.e. damping ratio or percent of critical damping). The damping increased to 0.7 % with a control factor of 2 and decreased to 0.2% with a control factor of -1. The eigenfrequency of the system remained nearly the same at 5.31 Hz for all test cases. This demonstrates, that the so-called dry wind concept can be utilized to reduce the stability of the system. Furthermore, the velocity proportional feed back control is well represented, as only damping is changing but not the eigenfrequency.

Now, the active control of the flutter suppression is tested together with shaker excitation, with varying control parameters p_F, presented in Figure 8. It can be observed that the damping is increasing with increasing control factor p_F. This is in contrast to equation (12), because the sign switches at the actuator. For this implementation, positive flap deflection commanded by the controller results in negative flap deflection at the actuator. Due to a phase shift imposed by the actuator, the deflected control surface is not fully velocity proportional. The delay results in a control surface acceleration response partially proportional to velocity of the wing (as desired) but also partially proportional to displacement of the wing (undesired). This means that the eigenfrequency increases with increasing control factor. The eigenfrequency of the reference system without control is identified at 5.33 Hz and the damping ratio is at 0.2 %. With a control factor of 0.5, the eigenfrequency increases to 5.42 Hz (undesired) and damping increases to 1.7 % (desired). Finally, a control factor of 1 further increases eigenfrequency to 5.56 Hz (undesired) and damping is increased to 2.5% (desired). A PI controller can be tuned such that the undesired eigenfrequency changes do not occur. For this study however, it is about the stabilization

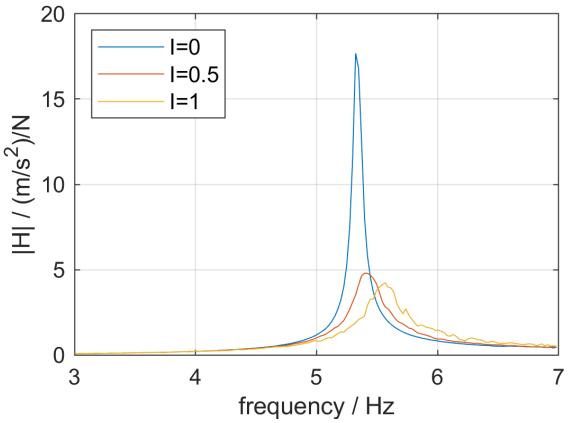

FIG 8. Measured transfer function for control surface control with shaker excitation

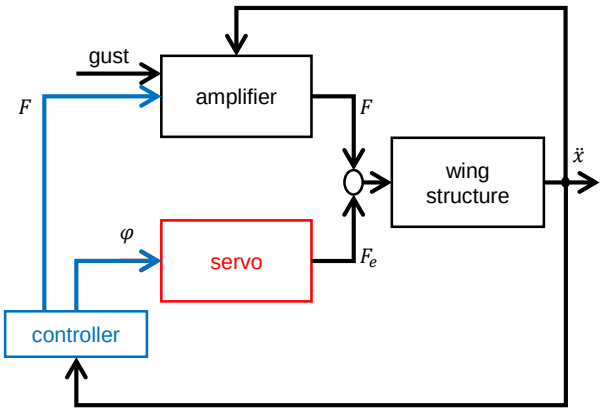

FIG 9. Comparison of simulation with experiment for shaker and control surface excitation

through increasing damping of the flutter suppression system, which is confirmed by these measurements.

3.3. Simulation Model

The simulation model is based on the equations (15) and (16) shown in the theoretical background with the identified parameters presented in the previous subsection. Figure 10 shows the comparison between the simulation model and the actual experiment. The top depicts the shaker excitation and it can be seen that the damping value is overestimated for the simulation. The bottom side depicts the result for control surface excitation and agreement here is better. However, the phase delay is not considered due to the actuator.

A full model is set up in Simulink with actuator model for the active flutter suppression and also the power amplifier model for the dry wind tunnel concept. A unique model is required however for the wing structure. The identified parameters from control surface excitation are taken in this case. The transfer function model can be expressed in terms of the modal parameters:

$$\frac{\ddot{x}}{u} = \frac{\Omega^2}{\omega_0^2 + 2iD\omega_0\Omega - \Omega^2} \quad , \tag{17}$$

where u is a summation of the inertial force due to the control surface excitation and the shaker excitation as stated in equation (1). Only one transfer function is used, because only one wing structure, as two input and one output system, is considered. Also, it can be seen that the denominator in equations (15) and (16) are the same. However, the control surface excitation depends on the angular control surface acceleration and requires a differentiation of the commanded control surface signal and multiplied by the residue. Due to the normalization of the equations, the force from the shaker is divided by the modal mass before it is put into the dynamic system. The resulting acceleration from the wing is fed back to the servo through an integral controller. The same applies to the power amplifier of the shaker. The acceleration from the wing is fed back to the shaker through an integral controller. With this, a complete model of the test setup is established. The free play however, is not implemented in the model. The resulting block diagram is shown in figure 9.

The commanded signal of the servo can be limited in velocity and deflection in order to represent the nonlinear behavior. This is implemented in the same way in the simulation model in Simulink as it is implemented in the real time controller to control the hardware in the physical laboratory setup. The advantage of the simulation model is however, that parameter studies can be performed to investigate the effect of such non-linear limitations on the overall performance without any risk.

4. STABILITY ASSESSMENT WITH NONLINEAR ACTUATOR

For the stability assessment, a 1-cos gust signal is sent to the shaker with a frequency of 5.3 Hz (i.e. duration of 0.189 s) and an amplitude of 20 N. The decay curve allows for the identification of the eigenfrequency as well as the damping and also to assess the stability. Shaker and control surface control parameters are varied systematically and independently in order to evaluate their effects on the system behavior in case of transient disturbance by gust excitation. In a next step, nonlinear behavior of the actuator is tested by limiting the commanded control surface signal.

Figure 11 shows the measured acceleration responses for different settings of the shaker control parameter p_I, where the flutter suppression is off. The yellow curve represents the reference system without control. Damping is increased with positive values of the control parameter, as can be seen in the purple and in the green curve. Correspondingly, damping is reduced with negative values of the control parameter. As one can clearly see, the wing can even be driven into an unstable region as shown with the blue curve of slightly increasing response

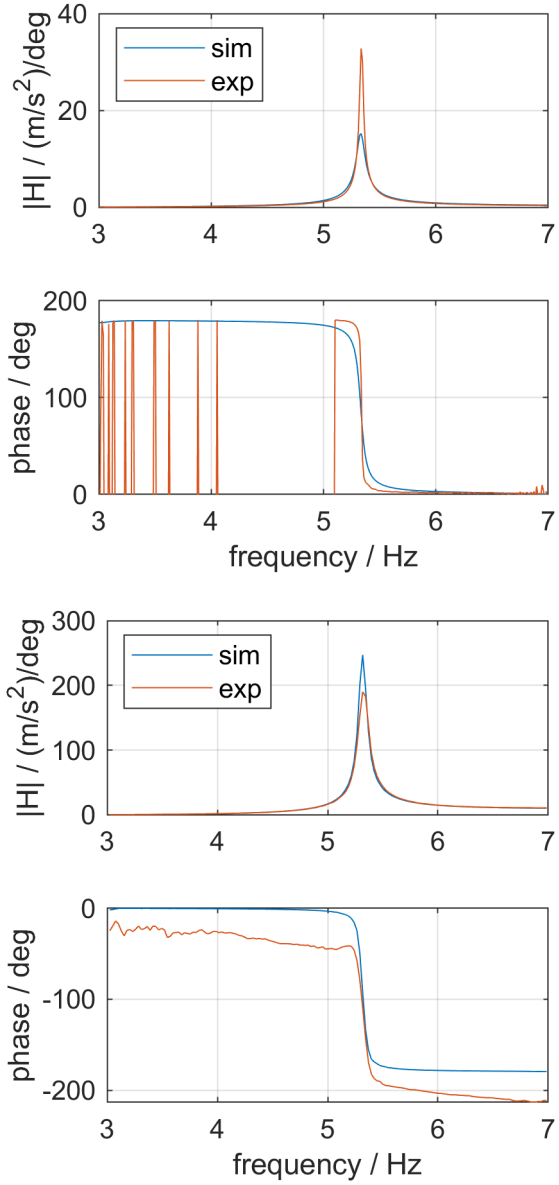

FIG 10. Comparison of simulation with experiment for shaker and control surface excitation

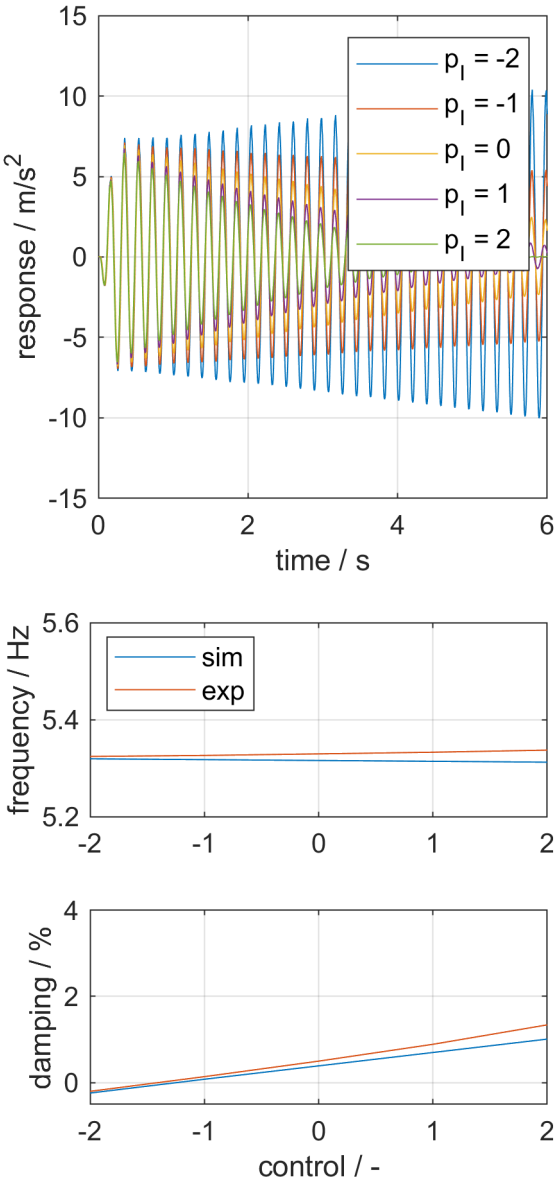

FIG 11. Variation of p_I only. Top: measured decay curves for different parameters; bottom: estimated poles.

amplitudes. The diagrams on the bottom show the damping and eigenfrequency estimates for the different control parameters. The red curves represent the identified results from measured responses shown on the top, while the blue curve represents identified results from simulated data with the same excitation. Both curves are in good agreement. It should be emphasized that this also applies to the prediction of the unstable region, where simulated and experimental findings are close. The eigenfrequency remains almost constant for all parameter settings, which is in good agreement with expectations.

Now, focus is on the effect of the control parameter of the control surface and the shaker control is off. Figure 12 shows on the top the decay curves for different parameter settings of the control surface control parameter. The blue curve represents the reference system without control. Increasing control parameters also increase the damping in this case, because the actuator is mounted in a way, that a commanded control surface deflection in positive direction results in a movement in negative direction. Nevertheless, it can be seen that the noise level also increases with increasing control gain. This results from high gain values for p_F which also amplifies the noise in the measured acceleration. Additionally, rattle occurs due to free play which also amplifies noise in the measured acceleration. The diagrams on the bottom present the eigenfrequencies and damping ratios identified from the decay curves in red. As one can see, the eigenfrequency is increasing with increasing control parameters. This has also been observed from the measured transfer functions in Figure 8. The damping is increasing significantly up to 3%. The results identified from simulated data is shown in blue. A depen-

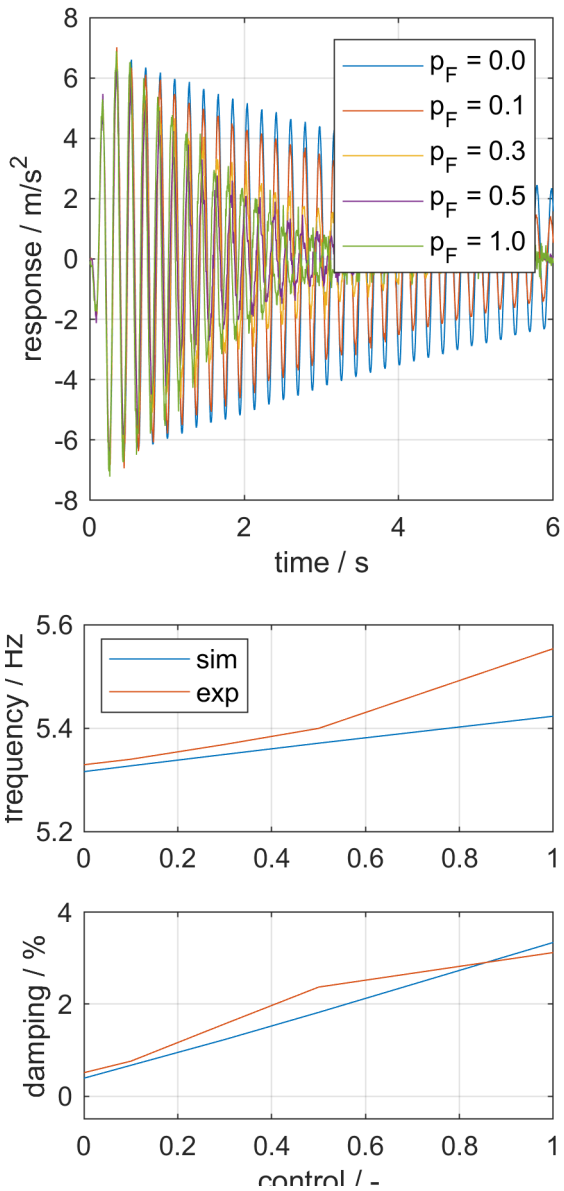

FIG 12. Variation of parameter p_F only. Top: measured decay curves for different parameters; bottom: estimated poles.

dency between damping and eigenfrequency with the control parameter is seen. This relationship is almost linear in case of simulated results, but not as clear in the experimental results. Nevertheless, both curves are in acceptable agreement, meaning that the prediction of the poles are reasonably accurate.

Due to the amplification of noise in case of high gains, the control parameter for the control surface control (i.e. active flutter suppression) was set to 0.5. The shaker control parameter (i.e. dry wind tunnel concept) is set to -2 in order to turn the system unstable. Figure 13 shows the decay curves where both controls were enabled. The blue curve shows the unstable system, when the shaker control is turned on. One can observe the gust excitation and the growing amplitudes thereafter. After 7 seconds, the flutter suppression is being enabled which stabilizes the system.

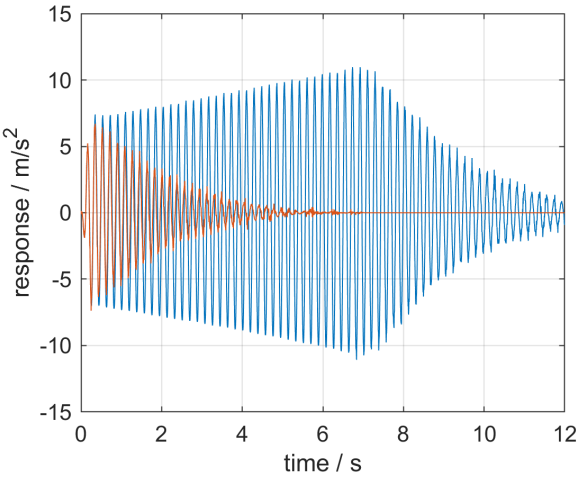

FIG 13. the control surface control is stabilizing the unstable system

One can observe that the amplitudes are shrinking afterwards. The red curve shows the gust response when both controls are enabled right from the beginning. This demonstrates that the actively controlled control surface is able to stabilize the unstable system.

So far, the concept has been demonstrated on a linear system with linear control law. In a next step, nonlinear behavior of the control surface is simulated experimentally by limiting the commanded signal to the servo. First, the deflection is bounded, then the deflection rate is limited. In these configurations, the control surface control gain p_F is again set to 0.5 and the shaker control gain p_I is set again to -2. These settings correspond to the the measurements shown in Figure 13. During the decay, a maximum deflection of the control surface of 5 deg is observed, the highest deflection rate during the decay is estimated at 250 deg/s and the maximum angular acceleration is approximately 9000 deg/s^2. Each nonlinearity is set individually, while the other parameter is not limited.

Figure 14 shows in the lower diagrams the pole estimates from decay curves for various maximum deflection levels. The red curve depicts the experimental results, whereas the blue curve presents the simulated results. Due to the limitations in the control surface deflection introduced artificially and the required additional computations to evaluate the reach of these limitations, the control performance reduces. The limitation of the angular deflection of the control surface can be observed from the angular measurement of the potentiometer in the second diagram of Figure 14. Even though the motion of the system is harmonic, the control surface deflection is no longer harmonic. Instead, it is a clipped harmonic function. If the allowed deflection of the control surface is further bounded to not more than 0.5 deg amplitude deflection, the wing becomes unstable, since the control surface is not able to damp the wing anymore. This can be seen in the red curve of the top diagram. However, if the deflection limited is relaxed a bit to 1 deg, the con-

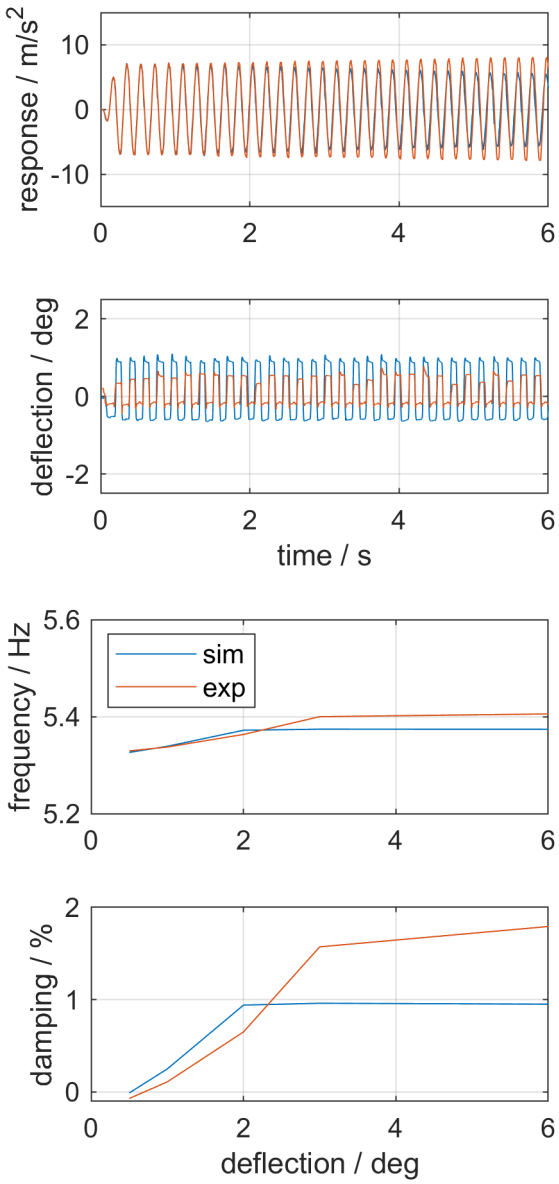

FIG 14. Variation of deflection limits. Top: decay curve and control surface deflection; bottom: poles estimates from decay curves.

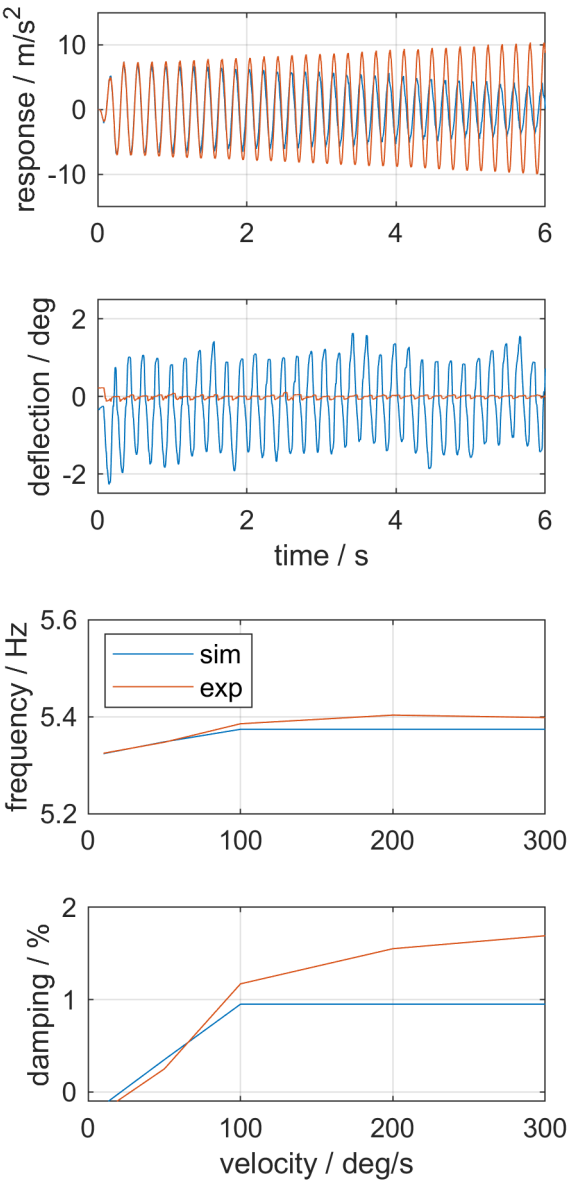

FIG 15. Variation of deflection rate limits. Top: decay curve and control surface deflection; bottom: poles estimates.

trol surface control is again able to stabilize the wing, as seen with the blue curve. The bottom plot shows, that this transition from stable to unstable is predicted correctly by the simulation.

Figure 15 shows the result for artificial limitation on the commanded deflection rate. The top diagrams show the acceleration time series at the top and the measured control surface deflection on the bottom. The blue curve has a nearly triangular shape, which is typical for saturation of the deflection rate. On the top plot, it is seen that this is enough to stabilize the system. The deflection rate was limited to 50 deg/s in this case. After further reduction of the maximum deflection rate to 10 deg/s, the wing turned unstable, as shown in the red curve in the top plot. The second plot shows that the control surface was almost not moving, possibly due to the free play. The bottom plot shows that the transition to unstable was again well predicted in the simulations, although the actual free play in the experimental setup was not integrated in the simulation model.

5. SUMMARY AND CONCLUSION

In this paper, an approach to active flutter suppression using an actively controlled control surface has been investigated numerically and experimentally. In order to investigate this experimentally, the de-stabilizing effects of motion induced unsteady aerodynamic forces have been emulated with shaker excitation with an adequate controller and response measurements. In fact, the shaker excitation with real time control did not provide equivalent unsteady aerodynamic forces. To do this, the solution of an unsteady aerodynamic

model would be required. Nonetheless, the shaker with active control was able to affect the damping of the system and with proper setting of a control parameter, it can destabilize the system similar to the approach of a flutter point in a wind tunnel (but much cheaper).
While shaker excitation with active control was applied to change the eigenmodes of an aeroelastic system in the sense of dry wind tunnel testing, active control surface control was applied to increase the damping and to stabilize the aeroelastic system. This is an approach to active flutter suppression using an actively controlled trailing edge control surface. From the active control surface control, it has been observed, that it is perfectly possible to change the wings behavior in terms of frequency and damping. However, this has not been the main target in this work.
While in a wind tunnel test, the aerodynamic forces of a control surface are being used, it was a bit different in our test case in the absence of aerodynamics. The control surface acted on the wing through inertial forces instead of aerodynamic forces. This differs from real flutter suppression. Nonetheless, a controller was successfully designed to stabilize the wing, which was driven unstable by the shaker with active control.
Actuator performance is highly sensitive to the overall performance of an aero-servo-elastic system. Furthermore, actuators are dynamic systems by themselves and can be nonlinear due to performance limitations. In order to study the performance of an actively controlled aeroelastic system with nonlinear actuator, the commanded deflection angle of the control surface has been limited in terms of deflection and deflection rate. The nonlinearity was not due to performance limitation in the real actuator, but saturations have been applied to the command signals sent to the actuator. Consequently, the nonlinearity has been introduced artificially in the actuator control. But since real actuators have the same saturation effects, the behavior of the overall system should be representative.
A simulation model has been built by mathematical modelling of the experimental setup and identification of the necessary parameters. The results from simulations and experiment are in good agreement. The prediction of the nonlinear behavior works well for gust excitation.
The impact of deflection limitation and rate limitation on the controller performance has been investigated by means of damping ratio. Ultimate goal is the stabilization of an unstable system. The system has been driven slightly unstable by the shaker. By means of deflection, the control surface is able to keep the wing stable with a maximum deflection of 1 deg for the assessed test cases. For rate limitations, the commanded signal has been distorted until it changed from sinusoidal into triangular shape and it was still able to stabilize the wing. For both cases the predictions from simulations were also able to predict the response well.
The results also strongly depend on the amplitude of the gust excitation. Higher amplitudes will drive the system faster into its limits. This does not mean that the system becomes more unstable, where the damping ratio decreases but the flutter suppression needs to respond with higher control surface deflections which means that the control surface runs faster into its limitations. From this study, the deflection and deflection rate could be limited up to 20% of the commanded deflection.
The flutter suppression worked well and has been driven into its limits with artificially set boundaries of the actuator. It could be observed how the performance in terms of damping ratio varied for the flutter suppression. When the restrictions were too high, the flutter suppression was not able to put enough damping into the wing so that it stayed unstable.
The investigations in this case were done using the dry wind tunnel test concept. For a future project, real unsteady aerodynamics should be considered to model the flutter suppression correctly. In this case, aerodynamic forces of the control surface will be used to counteract flutter instead of inertial forces.

Contact address:

martin.tang@dlr.de

References

[1] Béla Takarics, Bálint Patartics, Tamás Luspay, Balint Vanek, Christian Roessler, Julius Bartasevicius, Sebastian J. Koeberle, Mirko Hornung, Daniel Teubl, Manuel Pusch, Matthias Wustenhagen, Thiemo M. Kier, Gertjan Looye, Péter Bauer, Yasser M. Meddaikar, Sergio Waitman, and Andres Marcos. Active flutter mitigation testing on the flexop demonstrator aircraft. In *AIAA Scitech 2020 Forum*, Reston, Virginia, 2020. American Institute of Aeronautics and Astronautics. ISBN: 978-1-62410-595-1. DOI: 10.2514/6.2020-1970.

[2] Julian Theis, Harald Pfifer, and Peter J. Seiler. Robust control design for active flutter suppression. In *AIAA Atmospheric Flight Mechanics Conference*, Reston, Virginia, 2016. American Institute of Aeronautics and Astronautics. ISBN: 978-1-62410-390-2. DOI: 10.2514/6.2016-1751.

[3] Martin Tang, Marc Böswald, Yves Govers, and Manuel Pusch. Identification and assessment of a nonlinear dynamic actuator model for controlling an experimental flexible wing. *CEAS Aeronautical Journal*, 12(2):413–426, 2021. ISSN: 1869-5582. DOI: 10.1007/s13272-021-00504-y.

[4] J.-M. Yun and J.-H. Han. Development of ground vibration test based flutter emulation technique. *The Aeronautical Journal*,

124(1279):1436–1461, 2020. ISSN: 0001-9240. DOI: 10.1017/aer.2020.36.

[5] Jie Zeng, Dallas Kingsbury, Erich Ritz, Ping-Chih Chen, Dong-Hwan Lee, and Marc Mignolet. Gvt-based ground flutter test without wind tunnel. In *52nd AIAA/ASME/ASCE/AHS/ASC Structures, Structural Dynamics and Materials Conference*, Reston, Virigina, 2011. American Institute of Aeronautics and Astronautics. ISBN: 978-1-60086-951-8. DOI: 10.2514/6.2011-1942.